CrossMark

ORIGINAL PAPER

Synthesis of nano-γ-Al$_2$O$_3$/chitosan beads (AlCBs) and continuous heavy metals removal from liquid solution

A. Shokati Poursani[1,2] · A. Nilchi[2] · A. Hassani[1] · S. Tabibian[3] · L. Asad Amraji[1]

Abstract In this work, synthesis of chitosan beads impregnated with nano-γ-Al$_2$O$_3$ (AlCB) was carried out. The characteristics of the synthesized adsorbent were obtained by using Brunauer Emmett and Teller technique and Scanning Electron Microscopy method. The use of AlCB in continuous removal of chromium, lead, nickel and cadmium ions from liquid solution was studied using fixed-bed column system. Bed depths and flow rate effects on breakthrough and uptake capacity of the adsorbent in column were also examined. Dynamic parameters of the adsorption were calculated by using bed depth service time (BDST) and Thomas models. In both models, the data were analyzed by error analyzing and combining the values of determined coefficient (R^2) from regression analysis. The adsorption capacities of AlCB in breakthrough were 158.33, 183.33, 63.33 and 31.67 mg/g for chromium, lead, nickel and cadmium, respectively. In addition, BDST model was found to be an acceptable kinetic model to describe the experimental data.

✉ A. Shokati Poursani
shokatipoursani@gmail.com

1   Department of Environmental Science, Graduate School of the Environment and Energy, Science and Research Branch, Islamic Azad University, Tehran, Iran

2   Materials and Nuclear Fuel Research School, Nuclear Science and Technology, P.O. Box 11365-8486, Tehran, Iran

3   Department of Agriculture and Natural Resources, Payame Noor University, P.O.Box 19395-3697, Tehran, Iran

List of symbols

C_0	Influent concentration (mg/L)
C_t	Effluent concentration at any t (mg/L)
K_{Th}	Thomas rate constant [mL/(mg.min)]
K_{AB}	BDST the kinetic constant (L/mmol h)
M	Mass of adsorbent (g)
N_0	Dynamic bed capacity (g/L)
N_b	Is dynamic removal capacity of the fixed-bed column (mmol/cm^3)
q_e	Is the equilibrium heavy metals uptake (mg/g)
Q	Volumetric flow rate (mL/min)
t_b	Time at breakthrough (h)
t	Bed service time (h)
U_0	Linear flow rate (cm/h)
V	Linear velocity of flow rate (cm/h)
Z	Bed depth (cm)

Introduction

The rapidly expanding industrial development accompanied by population and consumption growth has generated new challenges about heavy pollution loads to the natural resources (Shahabfar et al. 2012; Baghvand et al. 2010). Water resources can be polluted by different activities, such as industries (Shokati Poursani et al. 2015), agriculture (Boularbah et al. 2006), fuel consumption (Norouzi et al. 2015) and transportations (Maniquiz-Redillas and Kim 2014). Nickel, lead, cadmium, chromium and most of other heavy metals are not environment friendly when they released to the environment (Sheng et al. 2008; Matouq et al. 2015; Lu et al. 2015). Therefore, one of the efficient ways for metal ions removal from water and wastewater is

🖄 Springer

1460

Int. J. Environ. Sci. Technol. (2017) 14:1459–1468

non-biological treatment. Various techniques, including adsorption, chemical precipitation, ion exchange and reverse osmosis, yet have been applied for metal ions removal from aqueous solution (Lu et al. 2015). Seeking for effective, cheap and low waste adsorbents, the application of different adsorbents for this purpose has been increased recently (Xie et al. 2015). Suitable metal ions adsorbent preference for clean-up aqueous solution would be very important. Some metal ions adsorbents are carbon nanotubes, nanometal oxides, nanozeolite composites, polymers and polymer-metal oxides (Shokati Poursani et al. 2015). Nanometal oxides have a large capacity for metal ions adsorption, caused by their large surface area and oxygen bridges presence in their structures (Yamani et al.2012). In this case, the maximum sorption capacities of nano-γ-Al$_2$O$_3$ for adsorption of Cr^{6+}, Pb^{2+}, Cd^{2+} and Ni^{2+} were calculated to be 13.3, 6.0, 1.1 and 0.33 mg/g, respectively, at laboratory temperature and in batch experimental conditions (Shokati Poursani et al. 2015). The practical techniques for water and wastewater treatment are developed based on batchwise laboratory studies which make them applicable in industries (Lu et al. 2015; Yamani et al. 2012).

The efficiency and structure of powder adsorbents should be improved by synthesis in composite form (Pinho et al. 2015). Metal oxide composites can be synthesized with many different materials (Pinho et al. 2015). Chitosan is a natural-based polymer with superior features like environmental compatibility, biodegradability and nontoxicity and adsorption attributes (Pinho et al. 2015). The chitosan characteristics related to the deacetylation degree, acetyl groups distribution, the length of chain and distribution of molecular mass (Schmuhl et al. 2001). Chitosan, which is a deacetylated form derived from chitin, that it is the polysaccharine natural base and made up from D-glucose amine and N-acetyl-D-glucosamine that randomly distributed b-(1-4)-linked (Xie et al. 2015). Therefore, it is an ideal organic compound material to be used in water treatment processes; it could be developed in the shape of beads, films and treats in non-acidic solutions as a hydrogel. (Miller and Zimmerman 2010). The great prevalence of chitosan attributes to including many functional groups like amino (2-site) and hydroxyl groups (6-site) which are worked as active sites for adsorption of metal ions (Xie et al. 2015). Besides, application of chitosan has many advantages like environmental and economic benefits and biodegradable properties, which could be extracted from shellfish waste (Miller et al. 2011).

Recently, chitosan and its derivatives like; chitosan cross-linked, chitosan beads and composites, have been applied as adsorbents for metal ions and other pollutants removal from liquid solutions (Pinho et al. 2015). Razzaz et al. (2015) improved the chitosan-TiO$_2$ composite

nanofibrous and used it for lead and copper ions removal. Their study showed that the maximum adsorption capacities for lead were more than copper ions. Li et al. (2015) synthesized the chitosan-sulfhydryl functionalized graphene oxide composites and studied lead, copper and cadmium ions removal. They concluded that adsorption competitive capacity order was Cd (II) > Cu (II) > Pb (II). Microspheres based on chitosan-organic rectorite were synthesized and used for low-concentration copper and cadmium ions removal from liquid solution (Xie et al. 2015).Pinho et al. (2015) synthesized the deactivated carbon xerogels–chitosan composite and usage for the azo dye orange removal from aqueous solution. The synthesis of titanium oxide-impregnated chitosan beads (TICB) was carried out and used for arsenic ions removal by Miller and Zimmerman (2010) and Miller et al. (2011), and the synthesis of mixed metal oxide-impregnated chitosan beads (MICB) containing nanocrystalline Al$_2$O$_3$ and nanocrystalline TiO$_2$ has been performed for removal of arsenate ions from water by Yamani et al. (2012). Moreover, Xie et al. (2015) have reported the synthesis of magnetic microspheres based on chitosan-organic rectorite for removal of low-concentration metal ions. In all of these studies, chitosan composites were used for low-concentration metal ions removal in batch conditions, whereas it was necessary to apply them in a fixed-bed column for an economic and continue usage.

Bohart–Adams and Thomas model are prevalently applied in modeling of fixed-bed breakthrough curves in biosorption and environmental sorption researches (Zhou et al. 2015; Chu2010). Cr (VI) removal from electroplating wastewater by coconut coir pith was surveyed in a fixed-bed column by Suksabye et al. (2008) whom considered the bed depth and flow rate effects. In this review, the maximum adsorption of chromium(VI) ions on adsorbent was measured to be 201.47 mg/g. Continuous adsorption studies under the bed depth, flow rate and initial pollutant concentrations effects were carried out in order to remove methylene blue from liquid solution by jackfruit leaf powder as adsorbent (Uddin et al. 2009). In another study, continuous sorption condition in a column was used for As (III) removal from liquid solution by applying iron oxide-coated cement, as an adsorbent and the bed depth, flow rate and initial concentration effects were evaluated (Kundu and Gupta 2007).

The objective of this work was to synthesize AlCB, and investigate and optimize the adsorbent properties for chromium, lead, nickel and cadmium removal from liquid solution. The synthesized adsorbent used for continuous of metal ions removal in a fixed-bed column is schematically shown in Fig. 1.

As previously mentioned, the synthesized nano-γ-Al$_2$O$_3$ was described by sol–gel technique with precursor of 1,
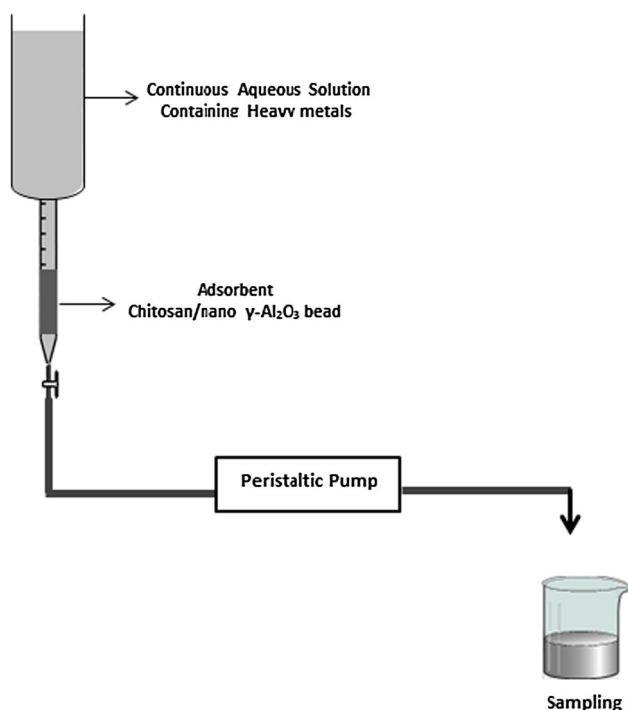
Fig. 1 Schema of fixed-bed column installation

2-epoxybutane, $AlCl_3$, $6H_2O$, absolute ethanol and deionized water (Shokati Poursani et al. 2015).

Materials and methods

All the selected agents were of analytical grade and obtained from Merck. Cd, Ni, Cr and Pb stock solutions were prepared by dissolving Cr_2O_7, $Cd(NO_3)_2 \cdot 11H_2O$, $Ni(NO_3)_2$ and $Pb(CH_3OO)_2 \cdot 3H_2O$ in deionized water. γ-Al_2O_3 nanoparticles had been synthesized in previous work (11.5 nm) (Shokati Poursani et al. 2015). Chitosan (medium molecular weight) was purchased from Orbital Company. A 1 M HNO_3 and NaOH solutions and a pH meter model 744 (Metrohm) were used for adjusting pH. Moreover, Gilson peristaltic pump model Miniplus Evolution was used to adjust the metal ions current to the column. Electrical Balance Model BP 221S (Sartorius), Ultrasonic (Viseclean), oven (Laboren), furnace (Nabertherm) and mixer model CH-4103-BOT Tmingen (HT Infors AG) were also used. Metals ions concentration analysis was done by using Inductivity Coupled Plasma (Optima 2000 DV).

Preparation and synthesis of nano-γ-Al_2O_3/Chitosan beads (AlCBs)

AlCBs were prepared by mixing chitosan 5 g with 0.1 M HCl (150 mL) by stirring (1000 rpm) until solution color

was changed to clear bright yellow (5 h). For preparing chitosan impregnated with γ-Al_2O_3, 1.67 g of γ-Al_2O_3 nanoparticle was added to the prepared solution, and mixing was continued to obtain a homogenous solution. A suitable nozzle added the obtained solution dropwise to NaOH solution (0.1 M) and mixed (100 rpm). After 24 h, the synthesized AlCB was rinsed and dried for 48 h at room temperature.

Adsorption studies

To determine the ideal pH values for sorption of metal ions by AlCB in a single ingredient, adsorption examinations were carried out by adding 3 g/L of AlCB to the solution with concentration of 20 mg/L of Cr^{6+}, Pb^{2+}, Cd^{2+} and Ni^{2+} ions. pH effect on ions sorption was investigated in the range of 3–6.5, at room temperature and contact time of 4 h. The concentration of metal ions before and after equilibrium sorption was analyzed using ICP. The uptake percentages of metal ions were calculated according to Eq. 1:

$$Up = \frac{(C_0 - C_e)}{C_0} \times 100 \tag{1}$$

where C_0 and C_e are initial and equilibrium concentrations of ions (mg/L), respectively. The results of optimum pH values for adsorption by AlCB are shown in Fig. 2.

Fixed-bed column adsorption experiments were carried out using AlCB packed into a glass column. The experiments were done by pumping the metal ions (chromium, cadmium, lead and nickel) solutions at optimum pH values for each metal through the column by using a peristaltic pump. All the experiments were carried out at room temperature. Metal ions samples were collected at specified intervals in the adsorptive process.

In dynamic experiments, 0.15 g of AlCB was placed in a column with 0.7 cm diameter and 15 cm length.

Fig. 2 The results of optimum pH values for adsorption by AlCB

1462

Int. J. Environ. Sci. Technol. (2017) 14:1459–1468
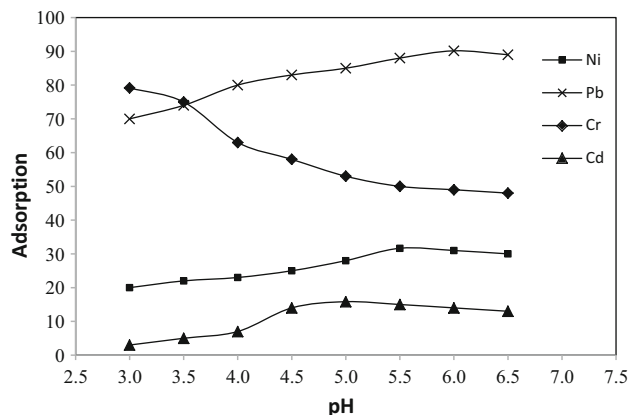
Afterward, in a single component, the aqueous solution containing each metal ion (concentration was 20 mg/L) was passed over the column. The effluent flow rate was adjusted at 0.25 mL/min by the peristaltic pump. The metal ions breakthrough curves were drawn by plotting the C/C_0 against time (t).

In order to describe the column behavior, two models, Thomas and bed depth service time (BDST) models, were used to fit the experimental data in the column. In Thomas model, the flow rate with variations of 0.25, 0.5 and 1 mL/min was adjusted, while metal ions concentration and bed depth were held fixed at 20 mg/L and 1.5 cm, respectively. In BDST model, the bed depth was adjusted at 1.5, 3, and 4.5 cm with 0.25 mL/min flow rate, while metal ions concentration was 20 mg/L. The behavior of metal ions in a column can be studied using a breakthrough curve, in terms of C_t/C_0 versus time t. In order to approve the fit model for the sorption system, it was necessary to analyze the data error and values of determined coefficient (R^2) from regression analysis (Han et al. 2007).

Characteristic of adsorbent (AlCB)

Scanning Electron Microscope (SEM)

The SEM images (taken by LEO, 440i) of synthesized AlCB are presented in Fig. 3. The shape of AlCB are very near to elliptical, with a mean diameter of about 450–500 μm (in dried beads). SEM images of these beads reveal the dispersion of nano-γ-Al$_2$O$_3$ particles (11.5 nm) on the surface of AlCB in surface morphology, especially on the shrinkage of the beads' surface occurred after drying. Increase in the dried bead-specific surface area may be a result of appearing shrinkage at the beads' surface after drying.

Pore volumes and surface areas by BET

AlCB-specific surface area was determined by nitrogen adsorption isotherms method. The surface area analysis was carried out through BET (model Quanta chrome NOVA 2200e). The comparison between the results of surface morphology-related parameters of γ-Al$_2$O$_3$ and AlCB is presented in Table 1. The total pore volume and specific surface area in nano-γ-Al$_2$O$_3$ particle are high in comparison with AlCB, while it is vice versa for average pore diameter sizes. The pore size distribution was obtained by Barrett–Joyner–Halenda method (BJH method revealed the mesoporosity). The pore size distribution against the specific surface area could be used for application of these beads inside the column in fixed-bed studies.

Results and discussion

Adsorption of metal ions on AlCB in fixed-bed column

Practical adsorption data in continuous studies in column were conducted to obtain the useful parameters such as dynamic sorption capacity and dynamic sorption efficiency from the breakthrough curve. Figure 4 shows the breakthrough curve [C/C_0 against time (t)] for metal ions sorption on the AlCB. The shape of breakthrough curve and the time for appearance of the breakthrough are the main elements determining the operation and dynamic response of the fixed-bed column (Nilchi et al. 2011a, b). It is evident that the capacity of adsorbent was raised at higher extent of AlCB masses. The volume of purified water at 50% breakthrough has risen when the AlCB mass increase from 0.15 to 0.45 g that conforms to 1.5–4.5 cm bed depth.

The general position of the breakthrough curve in the direct of the time axis depends on the column capacity with respect to the bed height, feed concentration and flow rate (Nilchi et al. 2011a). The dynamic capacity (DC) of the fixed-bed column is calculated by Eq. 2 (Nilchi et al. 2011a, b):

$$DC = \frac{C_0 v \int_0^t \left(1 - \frac{C}{C_0}\right) d_t}{M} \tag{2}$$

where v is volume flow rate (mL/min), t is time at a specified breakthrough (min), M is mass of AlCB sorbent (g), C is metal ions concentration in the effluent and C_0 is concentration of the influent. Two dynamic sorption capacities for the synthesized AlCB were calculated by evaluating the integral at 5 and 100% for each metal ion's breakthroughs (Table 2).
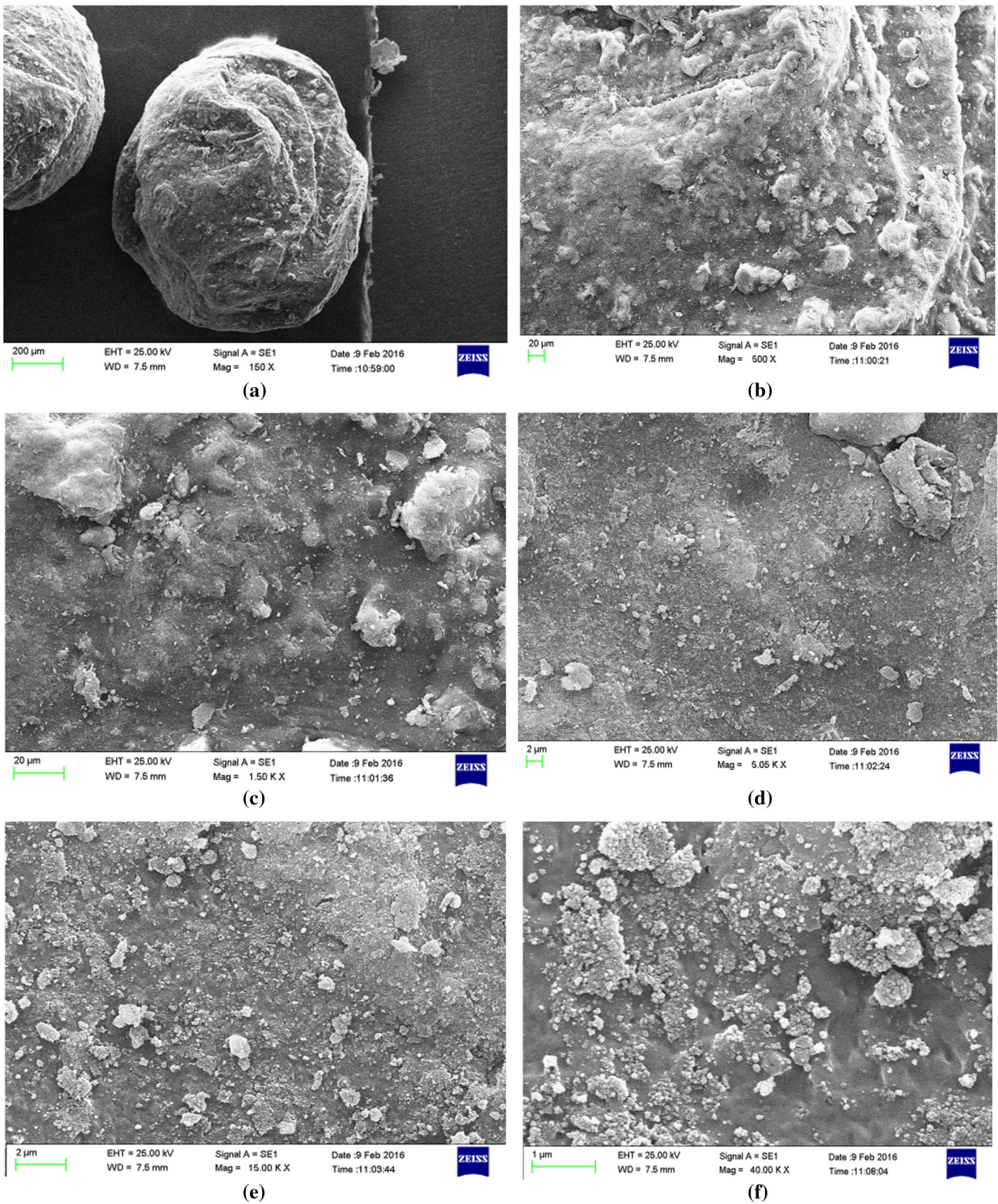
Equation 3 can calculate the efficiency of the adsorption column (E) (Nilchi et al. 2011a, b). The related data values are also indicated in Table 2.

$$E = \frac{Area1}{area1 + area2} \times 100 \tag{3}$$

where Area1 is the area above the curve from $C/C_0 = 0\%$ till $C/C_0 = 5\%$, and Area2 is the area above the curve from $C/C_0 = 5\%$ to $C/C_0 = 100\%$.

The mechanism of adsorption in AlCB was based on adsorption, the role of chemisorptions was very small due to the electrostatic repulsion between metal ions, and hydroxyl groups on the bead surface prevented chemisorptions (Miller et al. 2011). In AlCB, the nano-γ-Al$_2$O$_3$ particles located on the bead act as an oxidizing agent and amine and hydroxyl groups of chitosan (Yamani et al. 2012, Pinho et al. 2015) and also perform as a natural-

Fig. 3 SEM images of AlCB, **a** AlCB and **b–f** the surface of AlCB with different magnifications

1464

Int. J. Environ. Sci. Technol. (2017) 14:1459–1468

Table 1 BET analysis of nano-γ-Al$_2$O$_3$ and AlCB

Adsorbent	Average pore diameter (nm)	Total pore volume with diameter (cc/g)	Surface area (m^2/g)
γ-Al$_2$O$_3$	13.02	0.41	125.40
AlCB	15.84	0.45	11.32

Fig. 4 Breakthrough curves for **a** Cd, **b** Ni, **c** Pb and **d** Cr sorption on AlCB
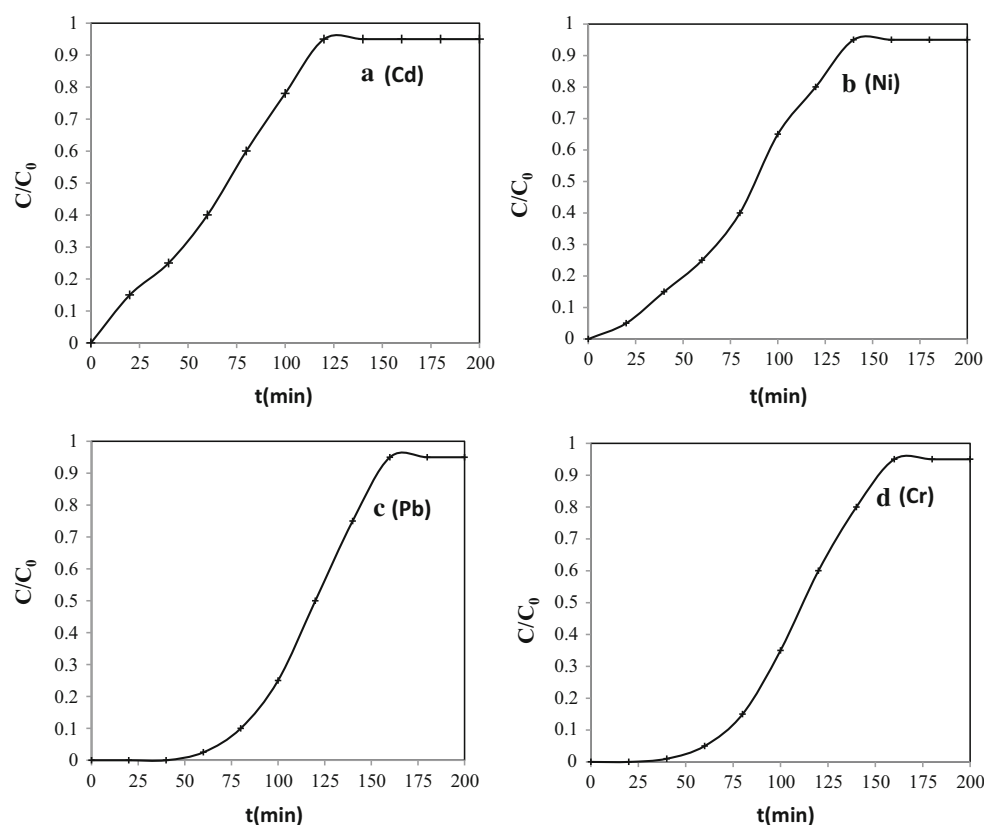
Table 2 Adsorption dynamic capacities in column experiment on AlCB adsorbent

Heavy metal	Flow rate (bed volume/h)	Dynamic capacity at 5% breakthrough (practical) (mg/g)	Dynamic capacity at 100% breakthrough (total) (mg/g)	Efficiency of adsorption column (%)
Cd	0.25	23.83	31.67	15.83
Ni	0.25	40.00	63.33	31.66
Pb	0.25	181.67	183.33	90.15
Cr	0.25	143.33	158.33	79.16

based material for sorption of metal ions (Miller and Zimmerman 2010; Gerente et al. 2007).

Breakthrough curve models

In order to describe the fixed-bed column behavior, two classic kinetic models, Thomas and bed depth service time (BDST) models, were used to fit the experimental data in the column.

Thomas model application

Thomas model for a fixed-bed adsorption column is presented by Eq. 4 as follows (Zhou et al. 2015):

$$C_t/C_0 = 1 \Big/ \left(1 + \exp\left(\frac{K_{th}q_e m}{Q}\right) - K_{th}C_0 t\right) \tag{4}$$

where K_{th} is the Thomas rate constant (mL/min.mg), q_e is the equilibrium metal ions uptake per g of the adsorbent

Int. J. Environ. Sci. Technol. (2017) 14:1459–1468

1465

(mg/g), m is mass of adsorbent (g) and C_0 and C_t are the effluent concentration of metal ions (mg/L) at time of 0 and t (mg/L), respectively. The value of C_t/C_0 is the ratio of effluent and influent metal ions concentrations (Baral et al. 2009; Futalan et al. 2011). The column kinetic coefficient Kth and adsorption capacity of the column qe can be obtained by plotting of C_t/C_0 against t at a given condition using the nonlinear regression method. The Thomas model was applied to the experimental data at various conditions. The linearized form of the Thomas model is presented by Eq. 5:

$$\ln\left(\frac{C_t}{C_0} - 1\right) = \frac{K_{th}q_e m}{Q} - K_{th}C_0 t \tag{5}$$

where plotting $\ln\left(\frac{C_t}{C_0} - 1\right)$ against t will determine the Thomas constants q_e and K_{th}.

Table 3 illustrates the results of parameters obtained from the Thomas model. The correlation coefficient values ranged from 0.97 to 0.99 and error percentages ranging from 0 to 4.55 indicate a good agreement between the experimental data and the column data generated using the Thomas model. Figure 5 shows a good agreement between the experimental and predicted data by the Thomas model. As seen in Table 3, the values of R^2 are all between 0.97 and 0.99. The relations of Q and K_{th} values are in reverse order in the column data obtained in varying flow rates. The rate constant K_{th} is observed to increase with the increase in flow rate. In other words, increase in the flow rate induces a decrease in the mass transport resistance, due to an increase in the molecules velocity and decrease in the boundary layer. The wet layer on the surface of adsorbent in the fixed-bed column can affect the mass transfer resistance (Yang et al. 2015).

In higher flow rates, the mass transfer of metal ions from the liquid layer to the adsorbent surface leads to less saturation of the adsorbent bed.

Table 3 Thomas model parameters at different flow rates for the removal of metal ions (Cd, Ni, Pb and Cr) by AlCB

Ions	Q (cc/min)	K_{th} (L/mg min)	q_e (mg/g)	R^2	e (%)
Cd	0.25	0.70×10^{-3}	26,568.89	0.96	1.84
	0.50	1.70×10^{-3}	4169.52	0.99	1.64
	1.00	2.10×10^{-3}	2227.78	0.98	0.14
Ni	0.25	2.40×10^{-3}	9082.99	0.92	4.55
	0.50	2.10×10^{-3}	5105.43	0.98	1.33
	1.00	2.00×10^{-3}	2945.53	0.99	2.91
Pb	0.25	2.70×10^{-3}	14,790.12	0.99	0.01
	0.50	2.50×10^{-3}	7794.77	0.99	0.01
	1.00	2.80×10^{-3}	4059.06	0.99	0.10
Cr	0.25	2.20×10^{-3}	13,585.18	0.98	0.71
	0.50	2.40×10^{-3}	7243.54	0.99	0.60
	1.00	2.90×10^{-3}	3787.57	0.99	0.10

BDST model application

The BDST equation was initially derived from the model described by Bohart–Adams, but Hutchins modified it. Due to the Bohart–Adams approach, at least nine column tests must be conducted to collect the required laboratory data. This model assumption was governed by the surface reaction between the adsorbate and the unused capacity of the adsorbent. It does not take into account the intra-particle mass transfer resistance as well as the external surface resistance where the adsorbate is directly adsorbed onto the surface of the adsorbent (Yang et al. 2015; Futalan et al. 2011). Eq. 6 (Yang et al. 2015) describes the Bohart–Adams model in a fixed-bed adsorption column:

$$\frac{C_t}{C_0} = \exp\left(K_{AB}C_0 t - K_{AB}N_0\left(\frac{Z}{U_0}\right)\right) \tag{6}$$

where Z is bed depth (cm), K_{AB} is kinetic constant (L/mmol.h), C_0 is influent concentration (mg/L), C_t is effluent concentration at any time t (mg/L), U0 is linear flow rate (cm/h) and N_0 is dynamic bed capacity (g/L).

Hutchin simplified the Bohart–Adams equation, presented a linear relationship between the bed depth and service time, and called it BDST model equation (Eq. 7). This model requires only three fixed-bed tests to collect the necessary data (Yang et al. 2015).

$$t_b = \frac{N_{bZ}}{C_0 V} - \frac{1}{K_{AB}C_0}\ln\left(\frac{C_0}{C_t} - 1\right) \tag{7}$$

where t_b is the service time at break through point (h), C_0 and C_t are initial and breakthrough solute concentration (mmol/L), respectively, N_b is dynamic removal capacity of the fixed-bed column (mmol/cm^3), KAB (L/mmol h) is the kinetic constant, and V (cm/h) is the linear velocity calculated by dividing the flow rate (Q) by the column section area. Equation 8 can be rewritten as in the form of a straight line (Yang et al. 2015):

$$t_b = aZ + b \tag{8}$$

where:

$$a = \text{slope} = N_b/C_0 V \tag{9}$$

$$b = \text{intercept} = -\frac{1}{K_{AB}C_0 \ln\left(\frac{C_0}{C_t} - 1\right)} \tag{10}$$

Thus, a linear plot of bed depth against time was drawn in order to determine the parameters of dynamic removal capacity and kinetic constant from the intercepts and slopes. The results of bed depth and service time at breakthrough point are plotted in Fig. 6.

The slope, intercept, R^2 and percentage of errors at breakthrough values were calculated in the same way by

1466

Int. J. Environ. Sci. Technol. (2017) 14:1459–1468

Fig. 5 Comparison of the experimental and predicted breakthrough curves for **a** cadmium, **b** nickel, **c** lead and **d** chromium removal by AlCB at different flow rates (initial metals concentration and bed depth were 20 mg/L and 1.5 cm, respectively)
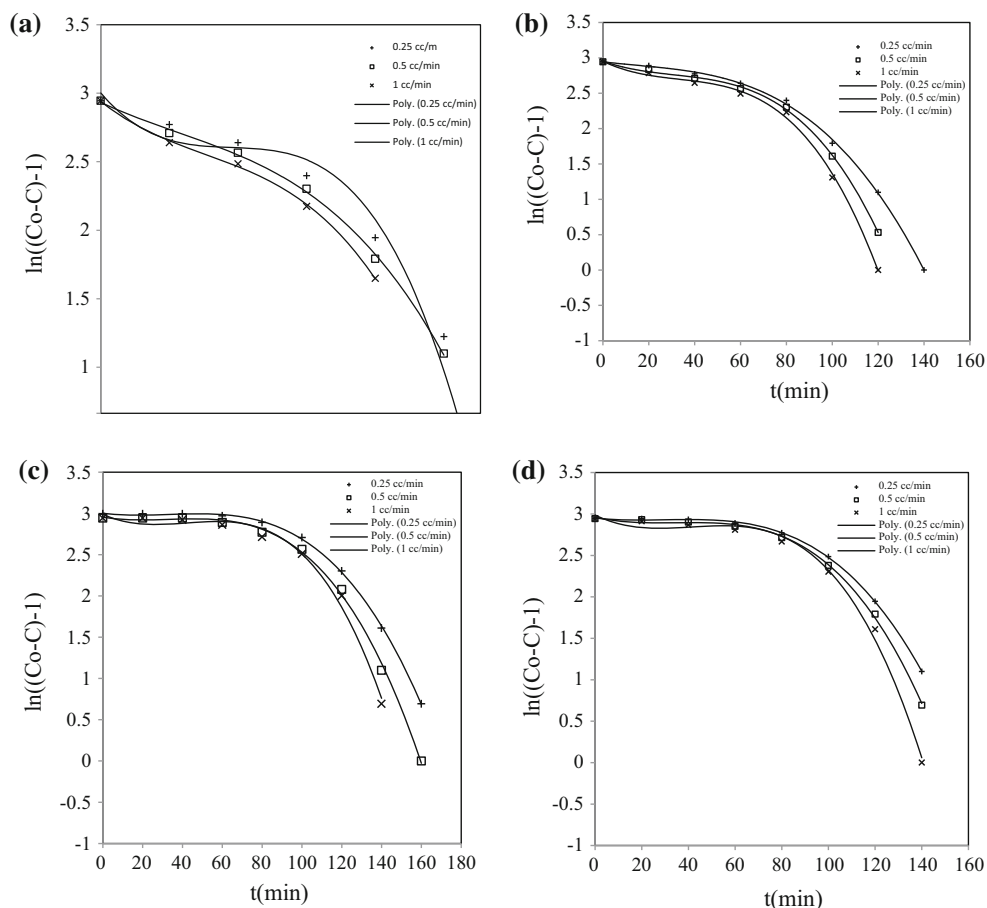
plotting service time versus bed depths (1.5, 3 and 4.5 cm). The results are listed in Table 4.

As seen in Table 4, the values of R^2 are between 0.97 and 0.99 and error percentages in the values are between 0.10 and 2.05. Error analysis of BDST model implies that all of the breakthrough curves are valid and could be used to describe the real values of the breakthrough curves.

Desorption of adsorbents

After continuous adsorption of the metal ions by adsorbents, it was necessary to regenerate them for further use. Regeneration was carried out by pumping 0.1 M HNO3 solution through the bed in the downward direction when the flow rate was 0.25 mL/min.

Conclusion

In this study, AlCB adsorbent was successfully synthesized and characterized by various techniques. The effect of some parameters, including pH, bed depths and flow rates on adsorption of chromium, lead, nickel and cadmium in a fixed-bed column was studied. It was found that the

optimum pH for sorption of cadmium, nickel, lead and chromium were 5, 5.5, 6 and 3, respectively. The obtained equilibrium data indicated that the maximum adsorption of metal ions by AlCB occurred at lower flow rates and higher bed depths. The adsorption capacity of the synthesized AlCB for the removal of arsenic and arsenate was higher than those reported. The adsorption capacity of nano-γ-Al_2O_3 for the removal of cadmium, nickel, lead and chromium followed the results of the previous studies (Shokati Poursani et al. 2015), and it was more than AlCB. However, the application of nano-γ-Al_2O_3 particles in continuous adsorption in column was not practical. Hence, AlCB would be an effective adsorbent in a continuous system for the removal of cadmium, nickel, lead and chromium from aqueous solution. Furthermore, the elliptical shape of AlCB would be an advantage in a fixed-bed column. The calculated dynamic capacities were 23.83 and 31.67 mg Cd/g sorbent, 40.00 and 63.33 mg Ni/g sorbent, 181.67 and 183.33 mg Pb/g sorbent and 143.33 and 158.33 mg Cr/g sorbent at 5 and 100% breakthroughs, respectively. In addition, according to the experimental data, influent flow rates such as bed depth and adsorbent quantity can affect the breakthrough curves. The BDST model was found to be better than the Thomas model in

Fig. 6 Comparison of the experimental and predicted breakthrough curves for **a** cadmium, **b** nickel, **c** lead and **d** chromium removal by AlCB at different bed depth (initial metals concentration and flow rate were 20 mg/L and 0.25 cc/min, respectively)
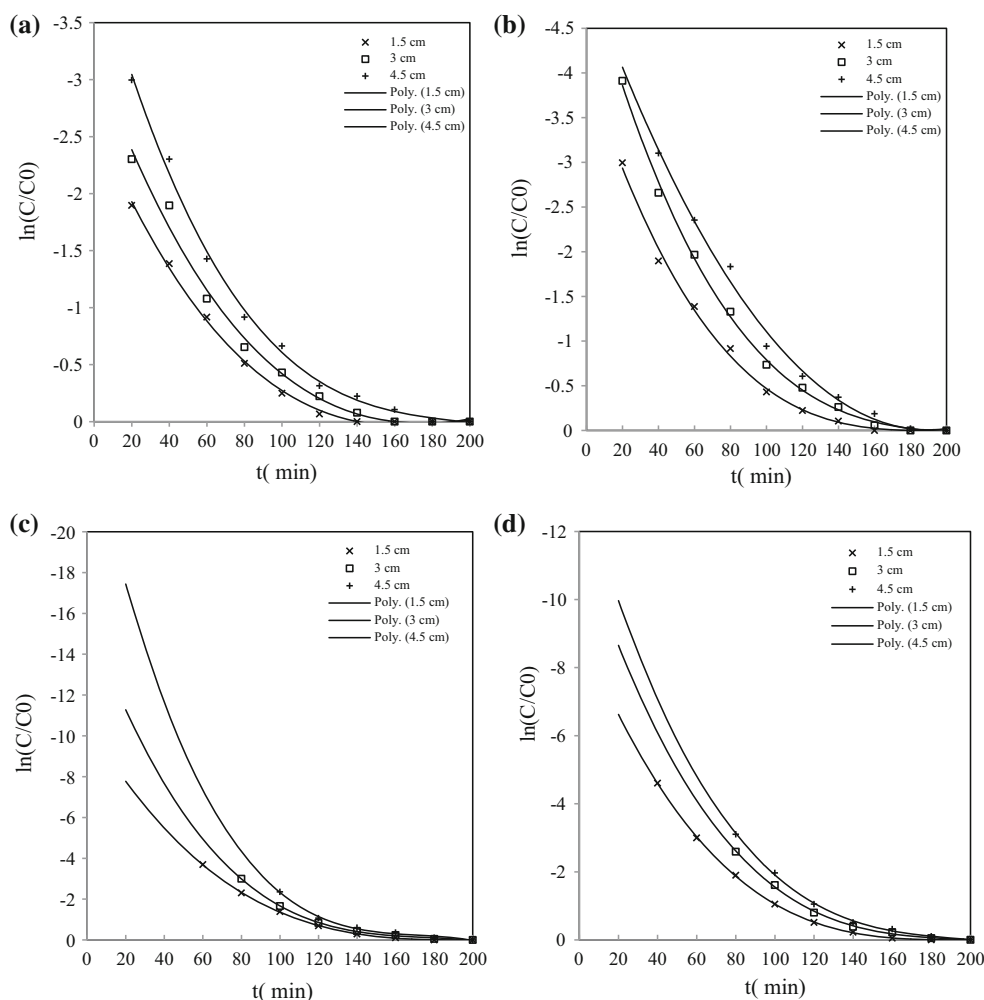
Table 4 BDST model parameters at different bed heights for the removal of metal ions (Cd, Ni, Pb and Cr) by AlCB

Ions	Bed depths (cm)	K_{BA} (L/mg min)	N_0 (mg/L)	R^2	e (%)
Cd	1.50	1.80×10^{-3}	108.49	0.99	0.47
	3.00	1.90×10^{-3}	135.61	0.99	0.37
	4.50	2.10×10^{-3}	222.78	0.98	0.85
Ni	1.50	2.20×10^{-3}	125.53	0.96	2.05
	3.00	2.20×10^{-3}	173.07	0.99	0.54
	4.50	2.00×10^{-3}	241.53	0.99	1.44
Pb	1.50	2.60×10^{-3}	153.91	0.98	1.06
	3.00	2.70×10^{-3}	216.33	0.99	0.03
	4.50	2.80×10^{-3}	405.01	0.99	1.07
Cr	1.50	2.50×10^{-3}	151.37	0.99	0.10
	3.00	2.60×10^{-3}	212/30	0.99	0.10
	4.50	2.90×10^{-3}	378.75	0.99	0.20

describing the behavior of metal ions removal by AlCB in whole breakthrough curves. The metal ions desorption from AlCB was also successfully carried out by 0.1 M HNO3 solution. The synthesized AlCB improved the adsorptive capabilities of nano-γ-Al$_2$O$_3$ for cadmium, nickel, lead and chromium. Finally, it can be concluded that, the high specific surface area of nano-γ-Al$_2$O$_3$, multiplies the active sites and specific surface area of AlCB.

1468

Int. J. Environ. Sci. Technol. (2017) 14:1459–1468

References

Baghvand A, Nasrabadi T, Bidhendi GN, Vosoogh A, Karbassi A, Mehrdadi N (2010) Groundwater quality degradation of an aquifer in Iran central desert. Desalination 260(1):264–275. doi:10.1016/j.desal.2010.02.038

Baral SS, Das N, Ramulu TS, Sahoo SK, Das SN, Chaudhury GR (2009) Removal of Cr(VI) by thermally activated weed Salvini-acucullata in a fixed-bed column. J Hazard Mater 161(2–3):1427–1435. doi:10.1016/j.jhazmat.2008.04.127

Boularbah A, Schwartz C, Bitton G, Aboudrar W, Ouhammou A, Louis Morel J (2006) Heavy metal contamination from mining sites in South Morocco: 2. Assessment of metal accumulation and toxicity in plants. Chemosphere 63:811–817. doi:10.1016/j.chemosphere.2005.07.076

Chu KH (2010) Fixed bed sorption: setting the record straight on the Bohart–Adams and Thomas models. J Hazard Mater 177(1–3):1006–1012. doi:10.1016/j.jhazmat.2010.01.019

Futalan CM, Kan CC, Dalida ML, Pascua C, Wan MW (2011) Fixed-bed column studies on the removal of copper using chitosan immobilized on bentonite. Carbohydr Polym 83(2):697–704. doi:10.1016/j.carbpol.2010.08.043

Gerente C, Lee VKC, Le Cloirec P, McKay G (2007) Application of chitosan for the removal of metals from wastewaters by adsorption mechanisms and models review. Crit Rev Environ Sci Technol 37(1):41–127. doi:10.1080/10643380600729089

Han R, Wang Y, Zou W, Wang Y, Shi J (2007) Comparison of linear and nonlinear analysis in estimating the Thomas model parameters for methylene blue adsorption onto natural zeolite in fixed-bed column. J Hazard Mater 145:331–335. doi:10.1016/j.jhazmat.2006.12.027

Kundu S, Gupta AK (2007) As (III) removal from aqueous medium in fixed bed using iron oxide-coated cement (IOCC): experimental and modeling studies. Chem Eng J 129(1–3):123–131. doi:10.1016/j.cej.2006.10.014

Li X, Zhoua H, Wu W, Wei S, Xu Y, Kuang y (2015) Studies of heavy metal ion adsorption on chitosan–sulfydryl functionalized graphene oxide composites. J Colloid Interface Sci 448:389–397. doi:10.1016/j.jcis.2015.02.039

Lu J, Li Y, Yin M, Ma X, Lin S (2015) Removing heavy metal ions with continuous aluminum electro coagulation: a study on back mixing and utilization rate of electro-generated Al ions. Chem Eng J 267:86–92. doi:10.1016/j.cej.2015.01.011

Maniquiz-Redillas M, Kim LH (2014) Fractionation of heavy metals in runoff and discharge of a storm water management system and its implications for treatment. J Environ Sci 26(6):1214–1222. doi:10.1016/S1001-0742(13)60591-4

Matouq M, Jildeh N, Qtaishat M, Hindiyeh M, Al Syouf MQ (2015) The adsorption kinetics and modeling for heavy metals removal from wastewater by Moringa pods. J Environ Chem Eng 3(2):775–784. doi:10.1016/j.jece.2015.03.027

Miller SM, Zimmerman JB (2010) Novel, bio-based, photoactive arsenic sorbent: TiO$_2$-impregnated chitosan bead. Water Res 44:5722–5729. doi:10.1016/j.watres.2010.05.045

Miller SM, Spaulding ML, Zimmerman JB (2011) Optimization of capacity and kinetics for a novel bio-based arsenic sorbent, TiO$_2$-impregnated chitosan bead. Water Res 45:5745–5754. doi:10.1016/j.waters.2011.08.040

Nilchi A, Saberi R, Azizpour H, Moradi M, Zarghami R, Naushad M (2011a) Adsorption of caesium from aqueous solution using cerium molybdate–pan composite. Chem Ecol 28(2):169–185. doi:10.1080/02757540.2011.629196

Nilchi A, Saberi R, Moradi M, Azizpour H, Zarghami R (2011b) b) Adsorption of caesium on copper hexacyanoferrate-PAN composite ion exchanger from aqueous solution. Chem Eng J 172(1):572–580. doi:10.1016/j.cej.2011.06.011

Norouzi S, Khademi H, Faz Cano A, Acosta JA (2015) Using plane tree leaves for bio monitoring of dust borne heavy metals: a case study from Isfahan, Central Iran. Ecolindic 57:64–73. doi:10.1016/j.ecolind.2015.04.011

Pinho MT, Silva AMT, Fathy NA, Attia AA, Gomes HT, Faria JL (2015) Activated carbon xerogel chitosan composite materials for catalytic wet peroxide oxidation under intensified process conditions. J Environ Chem Eng 3(2):1243–1251. doi:10.1016/j.jece.2014.10.020

Razzaz A, Ghorban S, Hosayni L, Irani M, Aliabadi M (2015) Chitosan nanofibers functionalized by TiO$_2$ nano particles for the removal of heavy metal ions. J Taiwan Inst Chem 58:333–334. doi:10.1016/j.jtice.2015.06.003

Schmuhl R, Krieg HM, Keizer K (2001) Adsorption of Cu(II) and Cr(VI) ions by chitosan: kinetics and equilibrium studies. Water SA 27(1):1–8. doi:10.4314/wsa.v27i1.5002

Shahabfar A, Ghulam A, Eitzinger J (2012) Drought monitoring in Iran using the perpendicular drought indices. Int J Appl Earth Obs Geoinf 18:119–127. doi:10.1016/j.jag.2012.01.011

Sheng XF, Xia JJ, Jiang CY, He LY, Qian M (2008) Characterization of heavy metal-resistant endophytic bacteria from rape (Brassica napus) roots and their potential in promoting the growth and lead accumulation of rape. Environ Pollut 156(3):1164–1170

ShokatiPoursani A, Nilchi A, Hassani AH, Shariat M, Nouri J (2015) A novel method for synthesis of nano-γ-Al$_2$O$_3$: study of adsorption behavior of chromium, nickel, cadmium and lead ions. Int J Environ Sci Technol 12(6):2003–2014. doi:10.1007/s13762-014-0740-7

Suksabye P, Thiravetyan P, Nakbanpote W (2008) Column study of chromium(VI) adsorption from electroplating industry by coconut coir pith. J Hazard Mater 160:56–62. doi:10.1016/j.jhazmat.2008.02.083

Uddin T, Rukanuzzaman M, Rahman Khan M, Islam A (2009) Adsorption of methylene blue from aqueous solution by jackfruit (Artocarpus heteropyllus) leaf powder: a fixed-bed column study. J Environ Manag 90(11):3443–3450. doi:10.1016/j.jenvman.2009.05.030

Xie M, Zeng L, Zhang Q, Kang Y, Xiao H, Peng Y, Chen X, Luo J (2015) Synthesis and adsorption behavior of magnetic microspheres based on chitosan/organic rectorite for low-concentration heavy metal removal. J Alloys Compd 647:892–905. doi:10.1016/j.jallcom.2015.06.065

Yamani JS, Miller SM, Spaulding ML, Zimmerman JB (2012) Enhanced arsenic removal using mixed metal oxide impregnated chitosan beads. Water Res 46:4427–4434. doi:10.1016/j.watres.2012.06.004

Yang Q, Zhong Y, Li X, Li X, Luo K, Wu X, Chen H, Liu Y, Zeng G (2015) Adsorption-coupled reduction of bromate by Fe(II)–Al(III) layered double hydroxide in fixed-bed column: experimental and breakthrough curves analysis. J Ind Eng Chem 28:54–59. doi:10.1016/j.jiec.2015.01.022

Zhou T, Lu W, Liu L, Zhu H, Jiao Y, Zhang S, Han R (2015) Effective adsorption of light green anionic dye from solution by CPB modified peanut in column mode. J Mol Liquids 211:909–914. doi:10.1016/j.molliq.2015.08.018